UNDISTURBED FLUID FLOW FOR IMPROVED MACROSCOPIC ESTIMATION OF DRAG FORCES ACTING ON CIRCULAR CYLINDERS

SATOSHI YOKOJIMA
Department of Mathematical and Systems Engineering, Shizuoka University, Hamamatsu, Japan, yokojima@shizuoka.ac.jp

TATSUHIKO UCHIDA
Department of Civil and Environmental Engineering, Hiroshima University, Hiroshima, Japan, utida@hiroshima-u.ac.jp

YUSUKE KAZEHAYA
Department of Mathematical and Systems Engineering, Shizuoka University, Hamamatsu, Japan

YOSHIHISA KAWAHARA
Department of Civil and Environmental Engineering, Hiroshima University, Hiroshima, Japan

ABSTRACT

A drag-force model is essential in practical predictions of flows around vegetation/forest/urban canopies, since it is too prohibitive to resolve details of the canopy elements and associated fluid motions, especially in environmental and geophysical applications. The model, however, has a serious difficulty inherent in its formulation: how one can specify the representative velocity? In ideal situations such as flows past an isolated obstacle, it is the velocity of the inflow and is easily available. In flows past multiple obstacles, on the other hand, a straightforward extension of the idea behind the ideal situations abovementioned leads to introduce undisturbed flow, which is the flow that would exist at an obstacle location in the absence of that obstacle but with all other obstacles present. Clearly, this undisturbed flow is unavailable unless a new system where the target obstacle is removed in actual is introduced. Therefore, most of the past studies used information of the fluid flow disturbed by the obstacle as the representative velocity. To improve the accuracy of this approach, one requires a methodology for estimating the undisturbed flow from the disturbed flow field. Here the undisturbed flow has been evaluated directly in fully resolved computations of a two-dimensional flow past circular cylinders and the fundamental properties of the flow are discussed.

Keywords: Undisturbed flow, Canopy flow, Drag-force model, Drag coefficient

1. INTRODUCTION

The use of a macroscopic drag-force model is essential in practical predictions of flows around vegetation/forest/urban canopies, since it is too prohibitive to resolve details of the canopy elements and associated fluid motions, especially in environmental and geophysical applications. The force $\mathbf{F}$ acting on a solid body immersed in a fluid of the drag coefficient C_{D} and the projected frontal area A is expressed in general by

$$\mathbf{F} = (1/2)C_{\mathrm{D}}\rho A|\mathbf{u}_{\mathrm{rep}}|\mathbf{u}_{\mathrm{rep}}, \tag{1}$$

where $\mathbf{u}_{\mathrm{rep}}$ denotes the speed of the object relative to the fluid. The force that the body exerts on the fluid per unit volume can be estimated by

$$\mathbf{f} = -\mathbf{F}/V = -(1/2)C_{\mathrm{D}}\rho\lambda|\mathbf{u}_{\mathrm{rep}}|\mathbf{u}_{\mathrm{rep}}. \tag{2}$$

This is the so-called drag-force model, where V denotes the volume of the body and $\lambda \equiv A/V$, the frontal area per unit volume, is referred to as the vegetation density for vegetation canopies.

The vegetation density λ, at least for geometrically simple canopies, can be determined easily and uniquely based on its definition. There is, however, no standard way to find a proper C_{D} even for simple arrays of cylinders that are typical laboratory models for vegetation. While various attempts

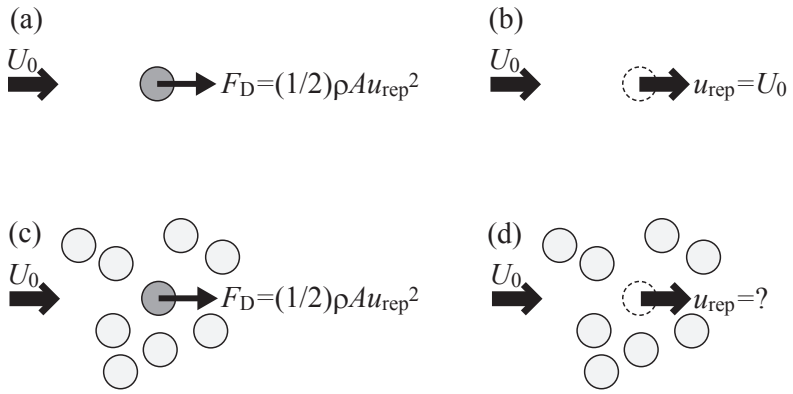

Figure 1. Undisturbed flow u_{un} required in eq. (1) to macroscopically predict the drag force acting on an isolated obstacle ((a),(b)) and on an obstacle in an array of obstacles ((c),(d)). The undisturbed flow is defined as the flow that would exist at an obstacle location in the absence of that obstacle, but with all other obstacles present. The undisturbed flow u_{un} is quite obvious in such ideal systems as (a) but is not at all in practical situations like (c).

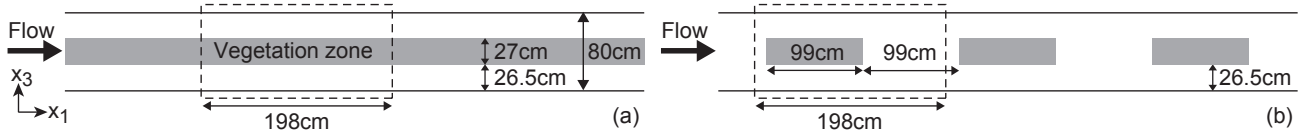

Figure 2. Schematic views of target flow and vegetation configurations: (a) Case 1; (b) Case 2. Dashed rectangle indicates the computational domain for the microscopic, fully resolved numerical simulations described in section 2.2.

have been made to obtain a better C_D for target flows of each study (e.g., Yokojima and Kawahara, 2015; Yokojima and Kawahara, 2016), this remains an open question.

Here particular attention has been paid not to the drag coefficient C_D but to the representative velocity $\mathbf{u}_{rep}$. In ideal situations such as flows past an isolated obstacle depicted in figure 1(a), $\mathbf{u}_{rep}$ must be the inflow U_0 (figure 1(b)). Next let us consider a practical situation where multiple obstacles exist as shown in figure 1(c). A straightforward extension of the idea behind figure 1(b) leads us to introduce 'undisturbed flow', which is defined as the flow that would exist at an obstacle location in the absence of that obstacle but with all other obstacles present (Akiki et al., 2017). Clearly the undisturbed flow at an obstacle location is unavailable unless a new system, where the obstacle is removed, is introduced (figure 1(d)), and hence it is important to appreciate that the macroscopic drag-force model, eq. (2), involves serious difficulties in its applications.

The objective of the present study is to examine the fundamental properties of the undisturbed flow in a two-dimensional flow past circular cylinders. The flow is reproduced numerically by using an immersed boundary method, where each of the cylinders, surrounding fluid motions and hydrodynamic force acting on the cylinder surface are fully resolved with no empirical formulas. This microscopic approach was referred to as preliminary analysis in Yokojima and Kawahara (2015, 2016). Undisturbed flow at a cylinder location is obtained directly by performing another fully resolved simulation of the flow where only the target cylinder is removed.

2. PHYSICAL AND NUMERICAL DETAILS

2.1 Physical details

The target problem is the vegetated open-channel flow studied by Yokojima et al. (2015). Figure 2 illustrates the schematic view of the flow through emergent vegetation canopies installed along the centerline of a 24 m long by 0.8 m wide flume with a bed slope of 1/555. Cylindrical bamboo stems of diameter $D = 3$ mm arranged in a lattice-type square pattern of stem-to-stem centerline spacing 3 cm are used as a laboratory model for vegetation. The resulting vegetation density λ is $1/30\,\mathrm{cm}^{-1}$.

Two specific vegetation configurations, Case 1 and Case 2, are focused here. In Case 1, the vegetation belt continuous in the streamwise x_1 direction is set along the centerline of the flume. Case 2 is an alternate arrangement in x_1 direction achieved by removing the vegetation in Case 1 at regular intervals.

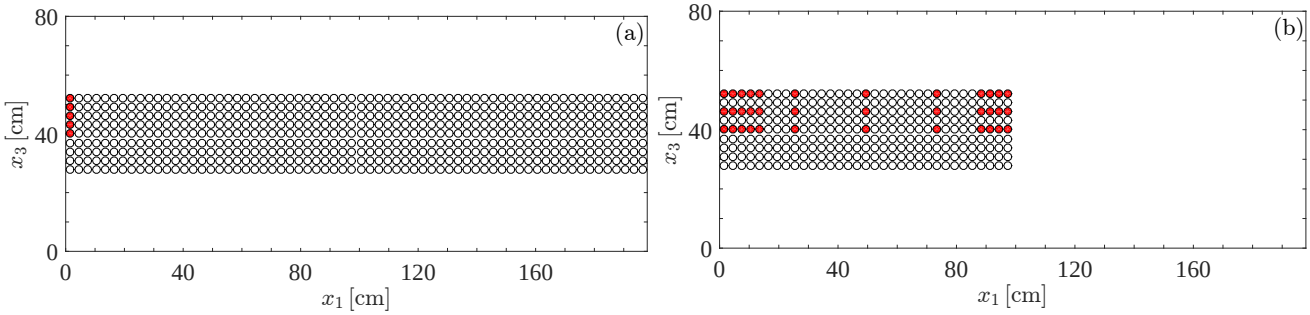

Figure 3. Computational domain and arrangement of circular cylinders for the present fully resolved numerical simulation: (a) Case 1; (b) Case 2. Periodicity is imposed in the streamwise x_1 direction. Each of the circular cylinders colored with red is removed to compute the undisturbed flow u_{un} at the cylinder location. For clarity, the cylinders are depicted larger than the actual size.

The flow discharge is set to be $9000\,\mathrm{cm}^3/\mathrm{s}$ in both cases, and the resulting mean water depth is 4.78 cm in Case 1 and 4.71 cm in Case 2. Under these conditions, the model plants are always emergent.

2.2 Numerical details

The experimental data of the target flow indicate that the mean flow structure is nearly uniform in the water-depth x_2 direction except in the vicinity of the flume bed (Yokojima et al. 2015). Based on the finding, we introduce a horizontally two-dimensional system whose schematic is presented in figure 3. The system represents the geometrical minimal unit in Case 2, and the periodicity of size 198 cm is imposed in the streamwise direction in both cases.

The stem Reynolds number Re_{D} based on the bulk mean velocity U_{b} and the cylinder diameter D is kept at 700 during the computations by directly adjusting the flow driving force. The Reynolds number is in accordance with the flow discharge experimentally observed in the vicinity of the free surface. It is well known that flow past an isolated circular cylinder accompanies three-dimensional structures in the wake when Re_{D} becomes larger than, say, 200 (Williamson, 1996). It is, however, unclear that how well the finding valid for an isolated cylinder is applicable to flows past an array of cylinders. We therefore use the two-dimensional system as zeroth approximation to the target flow.

An immersed boundary method (IBM) proposed by Uhlmann (2005) is employed for simulating the fluid motions around each circular cylinder and evaluating the hydrodynamic force acting on it. The reader is referred to Uhlmann (2005) for details of the IBM. A uniform grid spacing is employed for the streamwise x_1 direction. In the transverse x_3 direction, a non-uniform mesh distribution is used with fine grid spacings near the side walls and around the cylinders. The resulting spatial resolution within the vegetation zones is 12 grid points per diameter in both directions, which allows sufficient accuracy in reproducing cylinder wakes with no empirical formulas. The no-slip and impermeable conditions are imposed at the side walls as well as the cylinder surface.

2.3 Direct calculation of undisturbed flow

In Yokojima and Kawahara (2015, 2016), the microscopic, fully resolved numerical simulations of flow past circular cylinders described in section 2.2 have been carried out to estimate a proper C_{D} for the target flow. What they did is (i) to calculate the time-averaged drag force $\bar{F}_{\mathrm{D}}$ acting on each of the cylinders, (ii) to determine the representative velocity $\bar{u}_{\mathrm{rep}}$ to each of the cylinders from the time-averaged flow field, (iii) to evaluate the drag coefficient based on eq. (1), i.e., $C_{\mathrm{D}} = 2\bar{F}_{\mathrm{D}}/\left(\rho A \bar{u}_{\mathrm{rep}}^2\right)$, and (iv) to examine the applicability of the estimated C_{D} to the macroscopic numerical prediction of the target flow based on the drag-force model (eq. (2)). Yokojima and Kawahara (2015) equally applied the bulk-mean velocity U_{b} as the representative velocity $\bar{u}_{\mathrm{rep}}$ to all the cylinders, and referred to the estimated drag coefficient as $C_{\mathrm{D,global}}$. In Yokojima and Kawahara (2016), the fluid velocity seen by each of the cylinders (called as the approaching velocity $\bar{u}_{\mathrm{a}}$ in the literature) was estimated from the time-averaged flow field in the vicinity of the cylinder. The resulting drag coefficient based on $\bar{u}_{\mathrm{a}}$ was called as $C_{\mathrm{D,local}}$.

In the present study, the undisturbed flow is calculated at the location of each of the cylinders according to its definition described in section 1. The number of cylinders involved in the computational domain is 594 (= 9 rows times 66 columns) in Case 1 and 297 ($= 9 \times 33$) in Case 2. Hereinafter the cylinder i-th

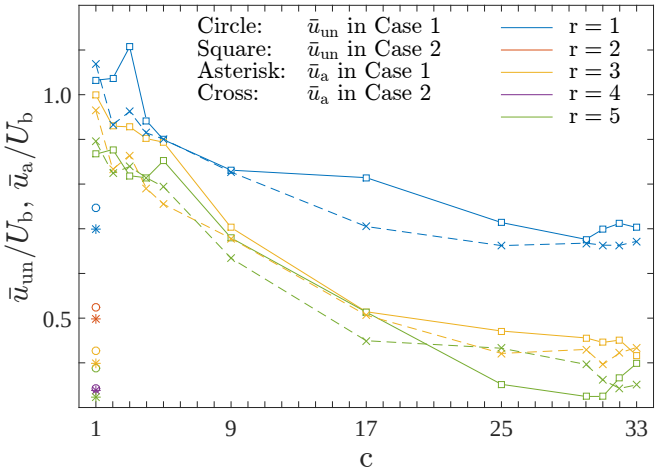

Figure 4. Distributions of undisturbed velocity u_{un} and approaching velocity u_a, normalized by the bulk-mean velocity U_b.

from the top (row) and j-th from the left (column) in figure 3 is referred to as 'ricj'. Note that obtaining the undisturbed flow at the locations of N cylinders requires N fully resolved simulations. As with Yokojima and Kawahara (2015, 2016), we expect eq. (1) holds at the time-averaged flow level. Then the number of cylinders that are statistically independent can be reduced to five ($= 5 \times 1$, r1c1, r2c1, r3c1, r4c1, r5c1, colored with red in figure 3(a)) in Case 1 due to the homogeneity in x_1 direction and the symmetry in terms of the flume centerline in the cylinder arrangement. Hence we performed all the five simulations, where the target cylinder colored with red in figure 3(a) was removed individually. In Case 2, since the homogeneity in x_1 direction does not hold up any more, the number of statistically-independent cylinders becomes 165 ($= 5 \times 33$), which is too many to perform all the simulations. Here, to capture the outline of the spatial distribution of the undisturbed flow within the vegetation zone, we focus on three cross sections in the transverse direction: i.e., r1, r3 and r5. In the streamwise direction, we choose 12 cross sections with particular attention to regions near the leading and trailing edges: i.e., c1, c2, c3, c4, c5, c9, c17, c25, c30, c31, c32 and c33. We therefore carry out 36 ($= 3 \times 12$) fully resolved simulations in total for Case 2. The undisturbed flow $\bar{u}_{un}$ at a cylinder location is obtained by double averaging procedure: both spatial averaging of the fluid velocity over the entire volume occupied by the target cylinder and temporal averaging.

3. RESULTS AND DISCUSSION

3.1 Undisturbed flow velocity and approaching velocity

Figure 4 presents the distributions of the undisturbed flow velocity $\bar{u}_{un}$. The abscissa c, which was introduced in section 2.3, denotes the location in the streamwise direction (column). In Case 1, $\bar{u}_{un}$ has a value of around $0.75U_b$ at r1 (i.e., on the side edge of the vegetation zone), is greatly reduced to about $0.5U_b$ at r2, and shows a gradually-decreasing trend as it gets inside further. On r1 cross section of Case 2, as it goes downstream, $\bar{u}_{un}$ first increases, reaches a maximum value of about $1.1U_b$ at c2, and then approaches around $0.7U_b$, which is close to $\bar{u}_{un}$ at r1 in Case 1. The rapid increase near the leading edge can be attributed to the presence of accelerated flow detouring around the vegetation patch. On r3 and r5 cross sections, $\bar{u}_{un}$ tends to decrease monotonically as it goes downstream. The velocity $\bar{u}_{un}$ on r5, however, started to deviate downward from $\bar{u}_{un}$ on r3 at c17, attained a minimum value of around $0.3U_b$, and at c33 has a value of $0.4U_b$, which is in close agreement with $\bar{u}_{un}$ at r3c33 and at r5 in Case 1.

The approaching velocity introduced in Yokojima and Kawahara (2016) was also plotted in figure 4. Figure 5 presents the time-averaged streamwise velocity profiles along the streamwise rows in a regular array of circular cylinders, passing the center of each cylinder, which was obtained from the fully resolved simulation without removing any cylinders. The approaching velocity $\bar{u}_a$ to the cylinder j-th from the left was defined by the maximum value of $\bar{u}_1$ between the (j-1)-th and j-th cylinders. It is noteworthy that the undisturbed flow at an obstacle location is unavailable unless a new system, where the target obstacle is removed like figure 1(d), is introduced. Therefore, it is also important to develop a method enabling us to estimate the undisturbed flow from the disturbed flow field. It can be seen in figure 4 that $\bar{u}_a$ captures the basic characteristics of $\bar{u}_{un}$ at least qualitatively and the maximum deviation is

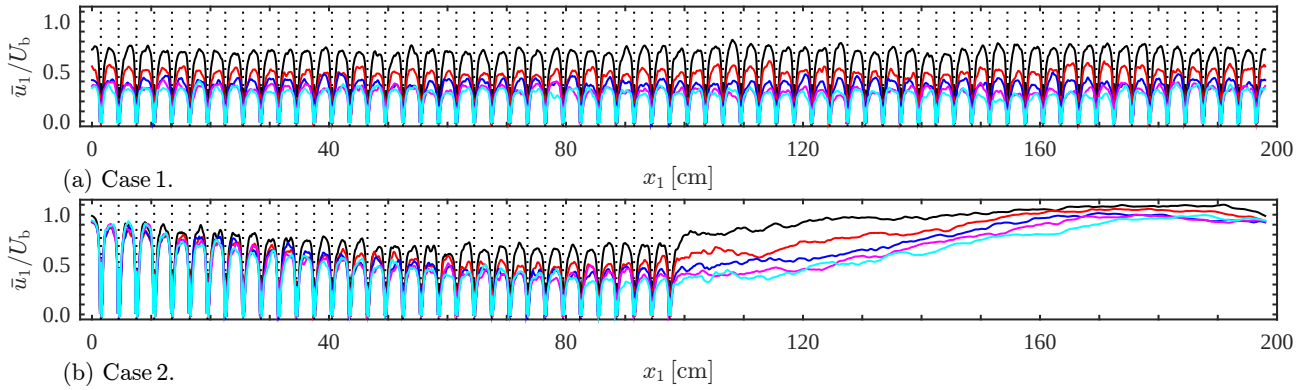

Figure 5. Time-averaged streamwise velocity profiles along the streamwise rows in a regular array of circular cylinders, obtained from the fully resolved simulation without removing any cylinders. The curves colored by black, red, blue, magenta, and cyan represent the velocity profiles along r1, r2, r3, r4, and r5 of the array, respectively. The black dots indicate the locations of the cylinder centers in the streamwise direction. This figure was reproduced from figure 2 in Yokojima and Kawahara (2016) for the readers' convenience purpose.

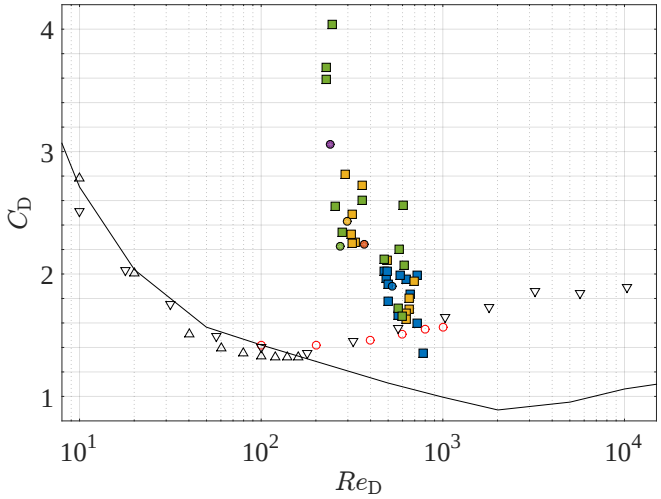

Figure 6. C_D–Re_D relation based on the undisturbed velocity $\bar{u}_{un}$. Solid line – an isolated circular cylinder (Finnemore and Franzini (2001)); open symbols – an isolated circular cylinder realized by 2-D CFD simulations (△, Park et al. (1998) - based on a body-fitted mesh; ▽, Tarukawa and Hirano (2008) - based on a body-fitted mesh; ◯, present - based on an immersed boundary method); filled symbols – array of circular cylinders (present, the meaning of each symbol is the same as those in figure 4).

around 10%. The drag coefficient C_D is, however, proportional of $\bar{u}_{rep}^2$ so that underestimating $\bar{u}_{rep}$ by a factor of 10% will cause overprediction of C_D by more than 20%. We will revisit this point in the next section.

3.2 Estimated drag coefficient

Figure 6 presents C_D–Re_D relation based on the undisturbed velocity $\bar{u}_{un}$ obtained at five locations in Case 1 (look at cylinders colored with red in figure 3(a)) and at 36 locations in Case 2 (figure 3(b)). A C_D–Re_D curve for an isolated cylinder from a textbook of Finnemore and Franzini (2001) and data obtained from a couple of 2-D CFD simulations are also included for comparative purposes. It is clear that C_D–Re_D relation for each cylinder in array of circular cylinders is deviated from that for an isolated circular cylinder even when C_D and Re_D are evaluated based on the undisturbed flow $\bar{u}_{un}$. It is therefore inappropriate to apply C_D–Re_D relation for an isolated cylinder to arrays of circular cylinders. It is also noteworthy that, with exceptions in regions near the side-edge/upstream-side area (e.g., r1c3) and around the middle-part/downstream-side area (e.g., r5c25 and r5c32), most C_D are in the range of 2.0 ± 0.5.

Finally, the distributions of estimated C_D within the vegetation zones, based on the undisturbed flow velocity $\bar{u}_{un}$ and the approaching velocity $\bar{u}_a$, are presented in figure 7. Note that $\bar{u}_{un}$ is available only at 36 locations in Case 2 and hence a linear interpolation was used to obtain $\bar{u}_{un}$ elsewhere.

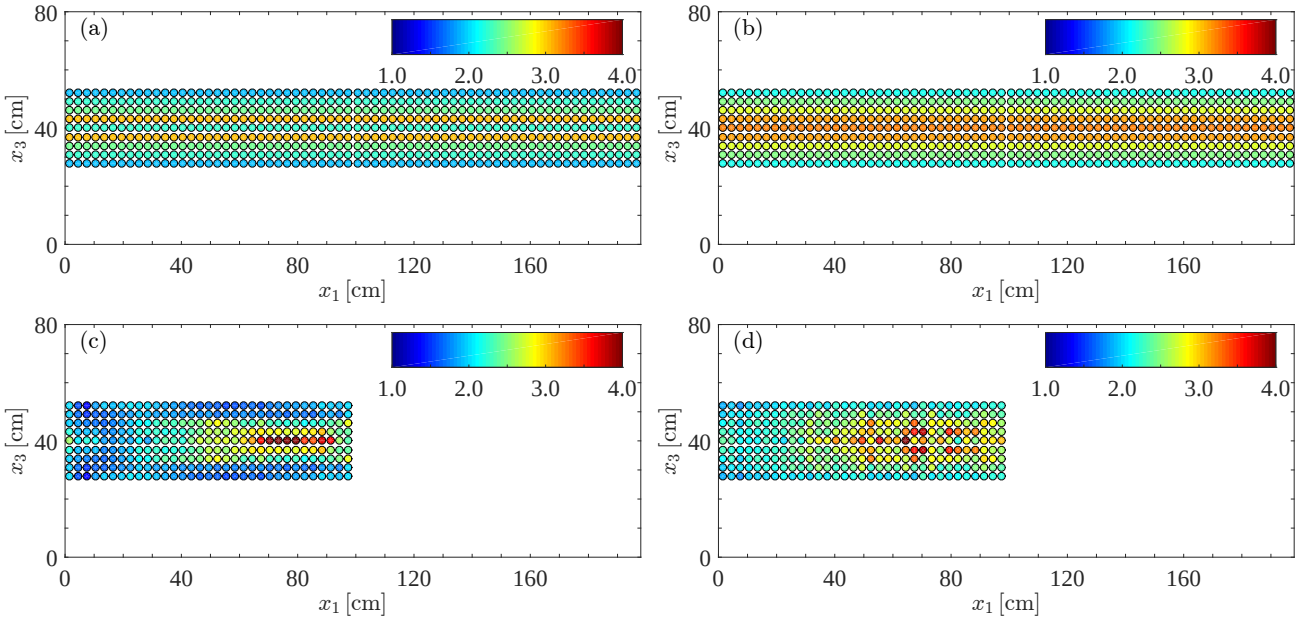

Figure 7. Estimated drag coefficient profiles (a) for Case 1 based on the undisturbed flow velocity $\bar{u}_{\mathrm{un}}$, (b) for Case 1 based on the approaching velocity $\bar{u}_{\mathrm{a}}$, (c) for Case 2 based on the undisturbed flow velocity $\bar{u}_{\mathrm{un}}$, and (d) for Case 2 based on the approaching velocity $\bar{u}_{\mathrm{a}}$. $1.90 \leq C_{\mathrm{D,ud,case1}} \leq 3.06$; $\langle C_{\mathrm{D,ud,case1}} \rangle = 2.39$; $2.17 \leq C_{\mathrm{D,a,case1}} \leq 3.23$; $\langle C_{\mathrm{D,a,case1}} \rangle = 2.71$. $1.36 \leq C_{\mathrm{D,ud,case2}} \leq 4.13$; $\langle C_{\mathrm{D,ud,case2}} \rangle = 2.13$; $1.79 \leq C_{\mathrm{D,a,case2}} \leq 4.15$; $\langle C_{\mathrm{D,a,case2}} \rangle = 2.46$. For clarity, the cylinders are depicted larger than the actual size.

Physically $\bar{u}_{\mathrm{un}}$ tends to be larger than $\bar{u}_{\mathrm{a}}$ that is affected by the no-slip and impermeable constraints on the cylinder surface, and it was mostly true as presented in figure 4. Therefore it can be expected $C_{\mathrm{D,un}} \equiv 2\bar{F}_{\mathrm{D}}/\left(\rho D \bar{u}_{\mathrm{un}}^2\right)$ generally becomes smaller than $C_{\mathrm{D,a}} \equiv 2\bar{F}_{\mathrm{D}}/\left(\rho D \bar{u}_{\mathrm{a}}^2\right)$. Figure 7 shows that this expectation indeed holds.

It was demonstrated in Yokojima and Kawahara (2016) that $C_{\mathrm{D,global}} \equiv 2\bar{F}_{\mathrm{D}}/(\rho D U_{\mathrm{b}})$ tends to underpredict the vegetation drag while $C_{\mathrm{D,a}}$, which was referred to as $C_{\mathrm{D,local}}$ in the article, basically overestimate the flow resistance. As mentioned above, the approaching velocity $\bar{u}_{\mathrm{a}}$ is a fluid velocity disturbed not only by the surrounding cylinders but also by the target cylinder itself to some extent. The bulk mean velocity U_{b} can be interpreted as a fluid velocity not disturbed by any cylinders. The undisturbed flow velocity $\bar{u}_{\mathrm{un}}$ falls between these two velocities and hence it is expected to resolve the abovementioned issue and to provide a proper resistance to the flow.

REFERENCES

Akiki, G., Jackson, T. L. and Balachandar, S. (2017). Pairwise interaction extended point-particle model for a random array of monodisperse spheres. *J. Fluid Mech.*, 813: 882–928.

Finnemore, E. J. and Franzini, J. B. (2001). Fluid Mechanics with Engineering Applications (10th edition). McGraw-Hill, New York.

Park, J., Kwon, K. and Choi, H. (1998). Numerical solutions of flow past a circular cylinder at Reynolds numbers up to 160. *KSME Int. J.* 12: 1200–1205.

Tarukawa, T. and Hirano, H. (2008). Computional fluid dynamics for around a circular cylinder with wide range Reynolds number. *Proc. National Symp. Wind Engrg.* 20: 66–71. (in Japanese)

Uhlmann, M. (2005). An immersed boundary method with direct forcing for the simulation of particulate flows. *J. Comput. Phys.* 209: 448–476.

Williamson, C. H. K. (1996). Vortex dynamics in the cylinder wake. *Annu. Rev. Fluid Mech.* 28: 477–539.

Yokojima, S., Kawahara, Y. and Yamamoto, T. (2015) Impacts of vegetation configuration on flow structure and resistance in a rectangular open channel. *J. Hydro-environ. Res.*, 9: 295–303.

Yokojima, S. and Kawahara, Y. (2015) Influence of model drag coefficient on LES prediction accuracy of vegetated open-channel flows. *E-proc. 36th IAHR World Congress*, The Hague, The Netherlands.

Yokojima, S. and Kawahara, Y. (2016) Drag coefficient distribution in LES of vegetated open channel flows. *Proc. 8th Int. Conf. Fluvial Hydraulics (River Flow 2016)*, St. Louis, MO, USA: 2240–2246.